analytical chemistry

Article

Cite This: Anal. Chem. 2019, 91, 4719−4726

pubs.acs.org/ac

Ultraviolet Absorption Cross Sections of KOH and KCl for Nonintrusive Species-Specific Quantitative Detection in Hot Flue Gases

Wubin Weng,[†] Christian Brackmann,[†] Tomas Leffler,[‡] Marcus Aldén,[†] and Zhongshan Li*[,†]

[†]Division of Combustion Physics, Lund University, P.O. Box 118, SE-221 00, Lund, Sweden

[‡]R&D, Strategic Development, Vattenfall AB, 814 26 Älvkarleby, Sweden

ABSTRACT: An understanding of potassium chemistry in energy conversion processes supports the development of complex biomass utilization with high efficiency and low pollutant emissions. Potassium exists mainly as potassium hydroxide (KOH), potassium chloride (KCl), and atomic potassium (K) in combustion and related thermochemical processes. We report, for the first time, the measurement of the ultraviolet (UV) absorption cross sections of KOH and KCl at temperatures between 1300 K and 1800 K, using a newly developed method. Using the spectrally resolved UV absorption cross sections, the concentrations of KOH and KCl were measured simultaneously. In addition, we measured the concentrations of atomic K using tunable diode laser absorption spectroscopy, both at 404.4 and 769.9 nm. The 404.4 nm line was utilized to expand the measurement dynamic range to higher concentrations. A constant amount of KCl was seeded into premixed CH_4/air flames with equivalence ratios varied from 0.67 to 1.32, and the concentrations of KOH, KCl, and atomic K in the hot flue gas were measured nonintrusively. The results indicate that these techniques can provide comprehensive data for quantitative understanding of the potassium chemistry in biomass combustion/gasification.

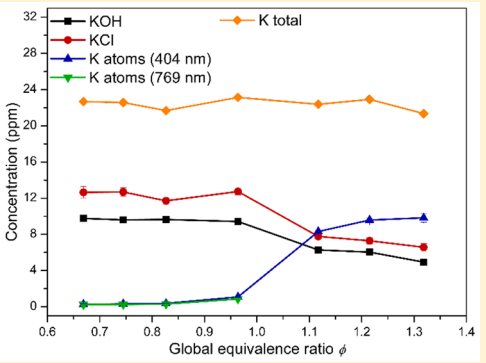

Biomass fuels, especially herbaceous, usually have a high content of potassium, which will be released as potassium hydroxide (KOH), potassium chloride (KCl), and atomic potassium (K) during combustion and gasification.[1−3] These potassium species, especially KCl, can cause severe operation problems of combustors and gasifiers, such as slagging, fouling, and high-temperature corrosion.[4] Thus, knowledge and understanding of the formation and release of potassium species is desired.

Optical diagnostics have been widely employed for concentration measurements of potassium species in many related studies.[5−8] Laser-induced breakdown spectroscopy (LIBS) was adopted to measure the total amount of potassium in flames,[9,10] while excimer laser-induced fragmentation fluorescence (ELIF) was used to detect the total amount of KOH and KCl compounds.[11,12] Planar laser-induced fluorescence (PLIF) has been used in measuring K atoms released from a burning biomass pellet.[8] To obtain reliable quantitative results, the application of absorption spectroscopic techniques is essential. Broadband UV absorption spectroscopy is a powerful tool for measurement of KCl and KOH,[13−15] and tunable diode laser absorption spectroscopy (TDLAS) has been applied to measure K atoms.[7,16] Collinear photofragmentation and atomic absorption spectroscopy (CPFAAS) was developed by Sorvajärvi et al.[17] for simultaneous detection of KCl, KOH, and atomic K.

In both UV absorption spectroscopy and the CPFAAS technique, absolute values of the UV absorption cross-section of KOH and KCl are indispensable in obtaining absolute concentrations. The UV absorption cross sections of KCl have been determined in previous investigations,[18−20] but these values are only available for temperatures up to 1200 K. The UV absorption cross sections of KOH and KCl at elevated temperatures, valid in combustion environments, are still lacking. Rowland and Makide[21] estimated the absorption cross sections of NaOH in flames based on the measurement of Daidoji,[22] but the values relied on the calculated amount of NaOH seeded into the flame, which introduced a severe uncertainty. Recently, Weng et al.[23] measured the UV absorption spectrum of KOH and KCl in flame environments, and the UV absorption cross sections were evaluated based on the KCl absorption data presented by Leffler et al.,[20] which were obtained at 1073 K. In the study of Weng et al.,[23] the influence of even higher temperature on the absorption cross-section values was assumed to be negligible.

In the present work, a new method is developed to directly evaluate the UV absorption cross sections of KOH and KCl in environments with temperatures of ∼1300 and 1800 K. Using the obtained cross sections, quantitative measurements of

Received: January 11, 2019
Accepted: March 5, 2019
Published: March 5, 2019

DOI: 10.1021/acs.analchem.9b00203
Anal. Chem. 2019, 91, 4719−4726

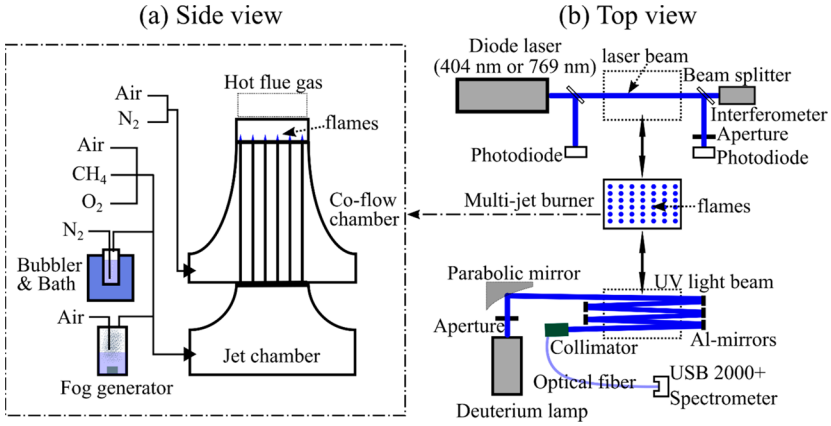

Figure 1. Schematic of (a) the setup for the burner system, and (b) the TDLAS system and the UV absorption system with the burner (top view).

Table 1. Flame Conditions

	Gas Flow Rate (sL/min)						
	Jet Flow			Co-flow			
flame case	CH_4	air	O_2	N_2	air	global equivalence ratio, ϕ	gas product temperature, T (K)
Flame 1	2.66	17.34	1.89	6.95	11.61	0.67	1770
Flame 2	2.66	17.34	1.89	10.84	7.74	0.74	1750
Flame 3	2.66	17.34	1.89	14.21	4.37	0.83	1760
Flame 4	2.66	17.34	1.89	18.60	0	0.96	1790
Flame 5	3.05	17.11	1.86	13.95	0	1.12	1840
Flame 6	3.14	15.53	1.91	12.09	0	1.22	1890
Flame 7	3.23	14.16	1.93	9.30	0	1.32	1750
Flame 8	2.28	11.89	2.26	22.69	9.82	0.67	1390
Flame 9	2.09	10.90	2.07	26.51	10.66	0.63	1260
Flame 10	2.66	9.12	2.15	18.60	0	1.31	1470

potassium species were made in flames seeded with a constant amount of KCl, but with equivalence ratios varied from 0.67 to 1.32 and a post-flame temperature of ~1800 K. Comprehensive experimental data were obtained as a substantial improvement in the study of the potassium chemistry, compared to the previous research based on the measurement of K atoms[25,26] or the total amount of KCl and KOH.[15] The concentration variation with equivalence ratios is discussed. The chemical balance between potassium species in different flame environments is presented.

METHODOLOGY

Burner and Flame Conditions. Homogenous hot flue gas environments in a series of well-defined conditions are prepared using an in-house developed multijet burner,[27] which has a rectangular outlet 85 mm × 47 mm in size. As shown in Figure 1, the burner consists of two chambers, namely, the jet chamber and the coflow chamber. The jet chamber supplies premixed gases to 181 cone-shaped laminar flames stabilized on an array of jet nozzles, and the coflow chamber supplies coflow gases through a perforated plate with holes surrounding each premixed jet flame evenly. The temperature and composition of the mimicked hot flue gas can be controlled by adjusting the composition and flow rates of the inlet gases, which are controlled via well-calibrated mass flow controllers (Bronkhorst). The flame conditions used in this study are presented in Table 1.

The investigated flames have different global equivalence ratios and temperatures (cf. Table 1). The global equivalence ratio (ϕ) is calculated based on the composition of the total inlet gases, indicating whether the environment of the hot flue gas is oxidative ($\phi < 1.0$) or reductive ($\phi > 1.0$). The temperature of the hot flue gas was measured using two-line atomic fluorescence thermometry (TLAF), which will be described in the following section.

Water solutions with 0.5 mol/L of potassium carbonate (K_2CO_3) or 1.0 mol/L of KCl were prepared and seeded into the flames. A fog of the solution, generated by an ultrasonic generator, was transported by an air flow with a flow rate of 0.41 sL/min into the jet chamber and thus seeded into the premixed jet flames, together with the reactant gases. The K_2CO_3 or KCl in the fog was vaporized and decomposed as it passed through the flame front region, and gas-phase potassium species, mainly KOH, KCl, and atomic K, were formed in the hot flue gases. Chloroform ($CHCl_3$) was used as another source of chlorine in the hot flue gas, besides potassium chloride, to control the ratio between potassium and chlorine. Liquid chloroform was filled in a gas bubbler bottle stored in a temperature bath (PolyScience) regulated at 273 K. The chloroform vapor was transported by a nitrogen flow into the jet chamber with a known concentration (a vapor pressure of 0.0779 bar at 273 K).[28] Assuming that all chloroform was decomposed through the flame fronts,[29,30] the concentration of chlorine in the hot flue gas was calculated, and the value was controlled by adjusting the flow rate of the carrier gas.

Temperature Measurements. The temperature of the hot flue gas ~5 mm above the burner outlet was measured with the TLAF technique, and the results are presented in Table 1 with an uncertainty of ~3%.[31] The details of the TLAF technique

DOI: 10.1021/acs.analchem.9b00203
Anal. Chem. 2019, 91, 4719−4726

using In atoms have been described by Borggren et al.[31,32] The present study used a similar setup, which mainly consisted of three parts, i.e., the indium seeding system, the laser system, and the imaging system. For indium seeding, an indium chloride ($InCl_3$) solution was used in the same system employed for potassium seeding. After passage through the flame front, free In atoms were produced to be used as the temperature marker. The laser system consists of two external cavity diode lasers (Toptica, Models DL100pro and DL 100) controlled by two separate analog control units, each including a temperature control module (DTC 110) and a current control module (DCC 110). Two continuous-wave laser beams were produced at wavelengths 410 and 451 nm. Both lasers have a power of ~5 mW and a beam size of ~1 mm^2. The laser beams were overlapped using a dichroic mirror and passed through the hot flue gas at a height of ~5 mm above the burner outlet. The indium transitions, $5^2P_{1/2} \rightarrow 6^2S_{1/2}$ and $5^2P_{3/2} \rightarrow 6^2S_{1/2}$, were probed and the fluorescence at 451 nm was captured by an ICCD camera (Princeton Instruments, Model PI-MAX 3) through a band-pass filter (450 nm ±10 nm). Evaluating the fluorescence signal, a temperature profile above the burner outlet was obtained.

Concentration of Potassium Atoms. The concentration of K atoms was measured using the TDLAS system, based on the Beer–Lambert law:[7,16,33,34]

$$I(\nu) = I_n + I_e + I_0(\nu)\exp[-\alpha(\nu)] \quad (1)$$

where ν is the frequency of the light, $I_0(\nu)$ and $I(\nu)$ are the intensity of the light before and after passing through the absorbers, respectively, and I_n and I_e are the frequency-independent backgrounds from the detector dark current and broadband emission, respectively. It was found that the broadband emission I_e from the investigated methane flames was negligible, especially as our detector was placed ~1.5 m away from the flame and an aperture was used in the beam path. I_n was assumed to be constant and obtained under the condition without laser beam in the flame. The frequency-dependent absorbance, $\alpha(\nu)$, is proportional to the optical path length L and the number density N of K atoms:[7,35]

$$\alpha(\nu) = \sigma(\nu)LN \quad (2)$$

where $\sigma(\nu)$ is the absorption cross section at frequency ν, which can be expressed as

$$\sigma(\nu) = \frac{h\nu_0 B_{12}\chi(\nu, N, T)}{c} \quad (3)$$

where h is the Planck's constant, ν_0 the central frequency, B_{12} the Einstein absorption coefficient, c the speed of light, $\chi(\nu,N,T)$ the area-normalized line shape function, and T the temperature. The line shape function can be described by a Voigt profile in the atmospheric environment. The Einstein absorption coefficient B_{12} can be related to the Einstein spontaneous emission coefficient A_{21} and expressed as

$$B_{21} = \left(\frac{c^3}{8\pi h\nu^3}\right)A_{21} \quad (4)$$

$$B_{12} = \left(\frac{g_2}{g_1}\right)B_{21} \quad (5)$$

where g_1 and g_2 represent the degeneracy of states 1 and 2, respectively.

In the calculation of the number density of K atoms, first, the measured absorbance $\alpha^m(\nu)$ was obtained based on eq 1 using measured intensities. Then, according to eqs 2 and 3, a Voigt profile was used to fit the measured absorbance $\alpha^m(\nu)$. With the fitted absorbance $\alpha^f(\nu)$, the number density N can be derived by integrating over eq 2, and can be expressed as

$$N = \frac{c}{h\nu_0 B_{12} L}\int \alpha^f(\nu)\, d\nu \quad (6)$$

In the present study, the concentration of K atoms was measured using two TDLAS systems with tunable continuous-wave diode lasers centered at 769.9 and 404.4 nm. The schematic diagram of the TDLAS system is presented in Figure 1b.

In previous studies of potassium,[7,16,33,34] TDLAS with 769.9 nm lasers has been adopted in favor of its high sensitivity. In our 769.9 nm TDLAS system, the beam with a power of ~3 mW and a size of ~1 mm^2 was provided by an external cavity laser (Toptica, Model DL100). Similar to the TLAF system, an analog control unit was used to control the temperature and the current of the laser. In addition, a scan control module (SC 110) was used to scan the wavelength with a range over 35 GHz at a repetition rate of 100 Hz. The scanning range was monitored by a high-finesse confocal Fabry–Perot etalon (Topoca, Model FPI 100), and the intensity of the light was monitored by two photodiodes of the same model (Thorlabs, Model PDA100A). The laser beam passed through the hot gas at a height of ~5 mm above the burner outlet with a path length of 8.5 cm.

Typical scanning signals with and without K atoms are shown in the insets of Figure 2. They were used to derive the measured absorbance $\alpha^m(\nu)$ presented in the main graphs. For the measurement with low concentration of K atoms (Figure 2a), the fitted absorbance $\alpha^f(\nu)$ was obtained through the fitting of $\alpha^m(\nu)$, using a Voigt profile, which has a full width at half-maximum (fwhm) of 5.34 GHz, similar to values obtained by Qu et al.[16] and Schlosser et al.[33] The number density N was calculated based on eq 6, and the concentration was determined to be 0.05 ppm.

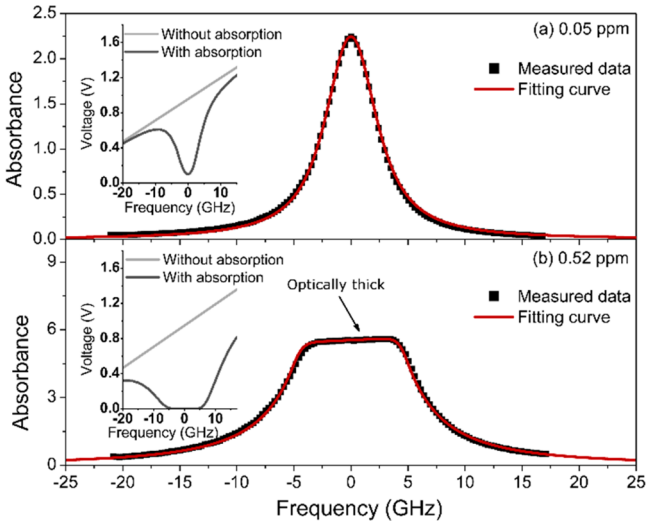

Figure 2. Absorption curves and Voigt function fittings of the $4^2S_{1/2} \rightarrow 4^2P_{1/2}$ potassium atom transition at 769.9 nm for concentrations of (a) 0.05 ppm and (b) 0.52 ppm. The measured curve in panel (b) is truncated due to strong absorption under optically thick conditions. The insets show the scanning signal as a function of laser frequency with and without potassium absorption.

DOI: 10.1021/acs.analchem.9b00203
Anal. Chem. 2019, 91, 4719–4726

However, as the concentration increases, an absorption spectrum with regions of complete signal extinction appears, indicating optically thick conditions, as shown in the inset of Figure 2b. Correspondingly, the absorbance peak was truncated and reached a maximum plateau level, which cannot be fitted by a Voigt profile. However, Qu et al.[16] reported that the Beer–Lambert law could still be applied to this condition, and the concentration of K atoms could be determined through a reconstruction of the absorption profile by fitting to the wings of the line profile. In the work of Qu et al.,[16] a corrected absorbance was used to fit the measured absorbance $\alpha^{m}(\nu)$ under optically thick conditions. In their correction, a simulated light intensity after absorption, $I^{f}(\nu)$, was derived based on eq 1, using a simulated absorbance $\alpha^{f}(\nu)$ with a Voigt profile from eq 2 and the light intensity without absorption $I_0(\nu)$. Then, under optically thick conditions, considering the response limit of the detector, values of $I^{f}(\nu)$ smaller than I_n were set to I_n, through which $I^{f}(\nu)$ was corrected to $I^{fc}(\nu)$, which was used to mimic the actual signal obtained from the detector. This correction process can be illustrated by the detector response curve shown in Figure 3 with a red dotted line. Then, the absorbance under optically thick conditions, $\alpha^{fc}(\nu)$, was derived from $I^{fc}(\nu)$ and $I_0(\nu)$, which was fitted to the measured absorbance $\alpha^{m}(\nu)$ through adjusting the absorbance $\alpha^{f}(\nu)$. In the present study, a similar correction process was used. However, a new correction equation was adopted for the conversion of $I^{f}(\nu)$ to $I^{fc}(\nu)$, to consider the nonlinear response of the detector to the very weak signal. The proposed nonlinear correction trend is shown in Figure 3, and the equation is expressed as

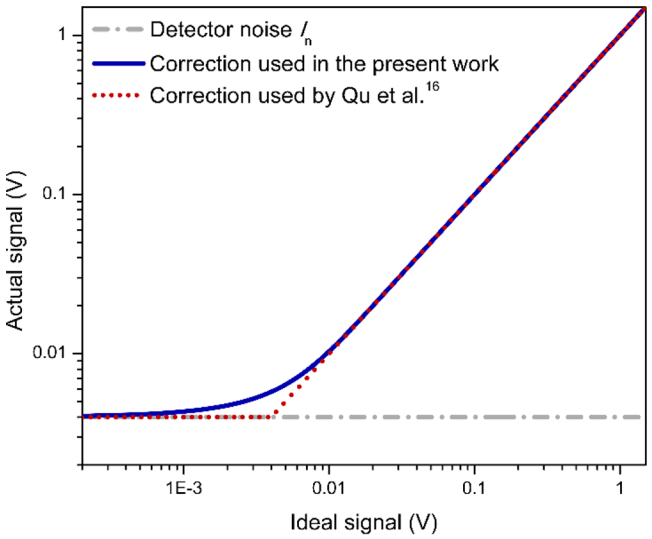

Figure 3. Proposed correction curve of the detector response used for TDLAS data analysis.

$$I^{fc}(\nu) = \ln[\exp[\beta I^{f}(\nu)] + \exp[\beta I_n] - 1]/\beta \quad (7)$$

where β is a constant to fix the curvature of the correction curve. As shown in Figure 2b, the $\alpha^{fc}(\nu)$ was well fitted to the measured absorbance $\alpha^{m}(\nu)$ with a suitable $\alpha^{f}(\nu)$ which was used to calculate the number density of K atoms using eq 6. The concentration of the K atoms in Figure 2b was determined to be 0.52 ppm.

It is clear that by using the method described by Qu et al.[16] for optical thick conditions, the measurement dynamic range can be increased dramatically, i.e., from 40 ppt to 40 ppm for a 1 cm path length for the 769.9 nm potassium $4^2S_{1/2} \rightarrow 4^2P_{1/2}$ line.[16] However, in the present study, the path length is 8.5 cm, and the concentration of K atoms can be over 20 ppm, which thus made it impossible to achieve a proper measurement using the 769.9 nm line, as most of the measured absorption peak would be truncated. Therefore, another TDLAS system probing the 404.4 nm $4^2S_{1/2} \rightarrow 5^2P_{3/2}$ transition was introduced. The 404.4 nm absorption has an Einstein spontaneous emission coefficient (1.16×10^6 s^{-1})[36] that is much smaller than the 769.9 nm line (3.75×10^7 s^{-1}),[36] which allows measurements of much higher concentrations (cf. eqs 2 and 3).

For the 404.4 nm TDLAS system, a beam with a power of ~5.5 mW and a size of ~1 mm^2 was provided by another external cavity laser (Toptica, Model DL100pro) controlled by an analog control unit. The wavelength was scanned with a range of ~21 GHz with a repetition rate of 100 Hz.

The scanning signals of the transmitted light with and without absorption by K atoms are presented in the insets of Figure 4,

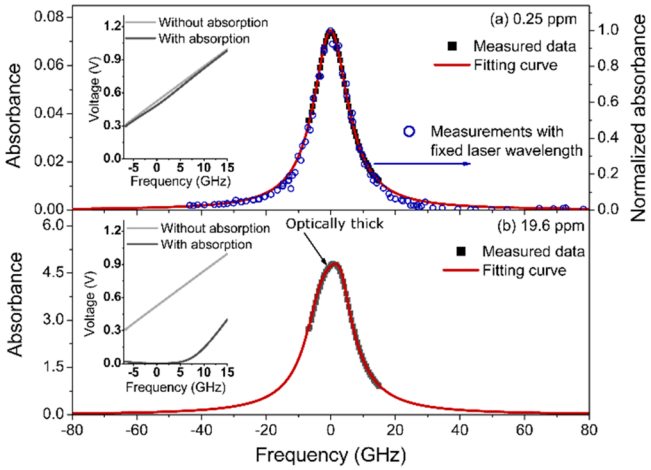

Figure 4. Absorption curves and the Voigt function fitting of the $4^2S_{1/2} \rightarrow 5^2P_{3/2}$ potassium atom transition at 404.4 nm for concentrations of (a) 0.25 ppm and (b) 19.6 ppm. The measured curve in panel (b) is truncated due to strong absorption under optically thick conditions. The insets show the scanning signal as the function of laser frequency with and without potassium absorption.

which were used to derive the measured absorbance profiles. It can be seen that the scanning range of 21 GHz cannot cover the entire absorption peak. For a low concentration situation, similar to the calculation process for the 769.9 nm case, the measured absorbance $\alpha^{m}(\nu)$ was fitted by the absorbance $\alpha^{f}(\nu)$, using a Voigt profile. The absorbance profile shown in Figure 4a has a full width at half-maximum (fwhm) of 13.3 GHz. In order to check the entire absorption profile, measurements with different fixed laser wavelengths were conducted, and the absorption values showed good overlap with the fitting curve from the data measured using laser scanning. Hence, the fitted absorbance $\alpha^{f}(\nu)$ were used in the concentration evaluation with eq 6. The concentration of K atoms in Figure 4a was determined to be 0.25 ppm, using this approach.

As the concentration of K atoms increased, the optical thick conditions occurred, as shown in the inset of Figure 4b. The corresponding measured absorbance $\alpha^{m}(\nu)$ with truncation of the absorption peak is shown in Figure 4b, and was well fitted by the absorbance after the correction on $\alpha^{f}(\nu)$ considering the optically thick absorption feature. Using the obtained $\alpha^{f}(\nu)$, the concentration of the K atoms in Figure 4b was determined to be

DOI: 10.1021/acs.analchem.9b00203
Anal. Chem. 2019, 91, 4719–4726

19.6 ppm. The introduction of the 404.4 nm TDLAS system thus further expanded our measurement dynamic range of K atoms, which fulfilled the requirement in this study.

Concentration of KOH and KCl. The concentrations of KOH and KCl were measured using UV absorption spectroscopy with the optical setup presented in Figure 1b. A deuterium lamp was used as the broadband UV light source and the light was collimated by a parabolic mirror to form a beam 10 mm in diameter through an aperture, and then guided to the hot flue gas region. With five UV-enhanced aluminum mirrors, the absorption path length above the burner was increased to 522 mm. Finally, the UV light is collected to a spectrometer (USB 2000+, Ocean Optics). To determine the path length and check the homogeneity over the line of sight, the distribution of KOH in the flue gas was visualized by laser-induced photofragmentation fluorescence, using the fifth harmonic of a pulsed Nd:YAG laser (Brilliant B, Quantel) at a wavelength of 213 nm.[11,12] A homogeneous distribution of KOH in the interrogated region was confirmed in this visualization measurement. As shown in Figure 5a, spectrally resolved absorbance

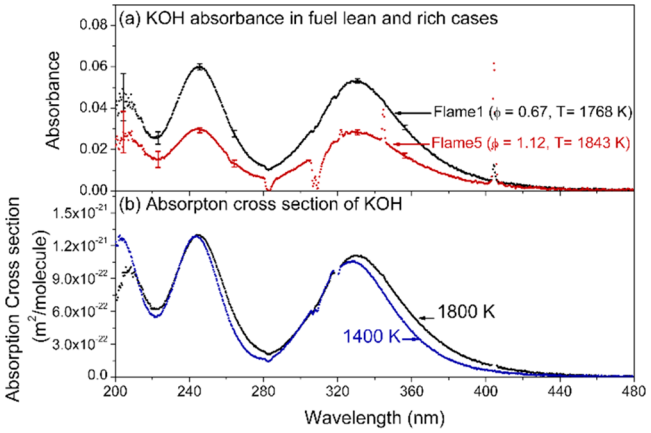

Figure 5. (a) Absorbance of KOH in the fuel lean and rich flames and (b) the derived UV absorption cross sections of KOH at different temperatures.

$A(\lambda)$ of different hot flue gases is obtained through the analysis of the collected spectrum using the Beer−Lambert law:[23]

$$A(\lambda) = -\ln\left(\frac{I_s(\lambda)}{I_0(\lambda)}\right) = N_A\sigma_A(\lambda)L \tag{8}$$

where $I_0(\lambda)$ and $I_s(\lambda)$ are the UV light intensity before and after the seeding of potassium to the hot gas, respectively, N_A is the number density of the alkali species in the hot gas, $\sigma_A(\lambda)$ is the absorption cross-section of alkali species, and L is the absorption path length. In obtaining the absorption spectral curve shown in Figure 5a (also in Figure 6), the USB spectrometer was set to have a gate width of 1 s, and 10 measurements were averaged for each case; hence, it took 10 s to obtain the UV spectra of KOH and KCl. In Figure 5a, the spectrum mainly consists of broadband absorption by KOH in the hot gas,[23] but the absorption lines of K atoms were also observed at wavelengths of 404, 345, and 322 nm. Some dips in the absorbance curve near 283 and 310 nm indicate the reduction of OH radicals in the hot gas with the seeding of potassium species.[23] UV absorption cross sections of potassium species, which are required to retrieve the concentration of KOH and KCl, are evaluated from the

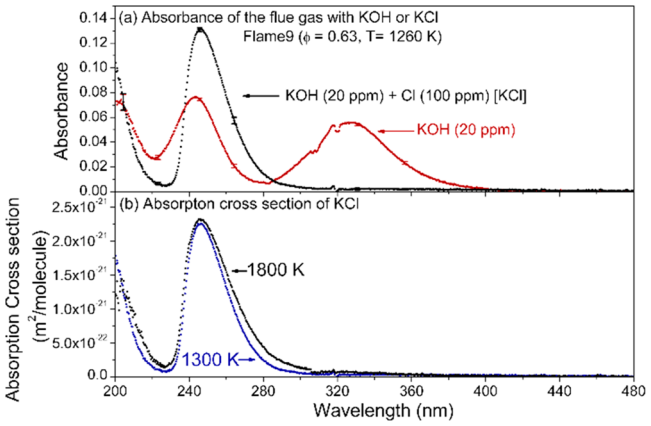

Figure 6. (a) Absorbance of KOH and KCl in Flame 9 with a global equivalence ratio of ϕ = 0.63 and a temperature of 1260 K and (b) the derived UV absorption cross sections of KCl at different temperatures.

absorbance data and presented in Figure 5b. The details of the evaluation process will be described in the following section.

RESULTS AND DISCUSSION

UV Absorption Cross Sections of KOH and KCl. In the present study, the UV absorption cross-section of KOH in a combustion atmosphere was determined. In this evaluation, a constant amount of K_2CO_3 was introduced into one fuel-lean flame and one fuel-rich flame. The potassium chemistry results in the generation of KOH and K atoms as the dominant potassium species in the hot flue gas.[24] In the fuel-lean case, KOH is the dominant species, whereas, in the fuel-rich case, nearly half of the potassium exists as K atoms. When changing from a fuel-lean flame to a fuel-rich flame, the increase of the concentration of K atoms will be equal to the reduction of KOH. Based on the measured K atom concentrations for the lean and rich cases, the absorption cross sections of KOH were evaluated using the measured absorbance difference of KOH from the UV absorption spectroscopy. Derived from eq 8, the evaluation process can be described with the following equation:

$$N_{\text{K-rich}} - N_{\text{K-lean}} = N_{\text{KOH-lean}} - N_{\text{KOH-rich}} = \frac{A_{\text{KOH-lean}}(\lambda) - A_{\text{KOH-rich}}(\lambda)}{\sigma_{\text{KOH}}(\lambda) \times L} \tag{9}$$

where N indicates the number density of K atoms and KOH molecules in different flame cases. $A(\lambda)$ indicates the absorbance of KOH in different flames. $\sigma_{\text{KOH}}(\lambda)$ represents the absorption cross-section of KOH and L indicates the optical path length. The subscripted prefixes "K" and "KOH" indicate the potassium species while the subscripted root words "rich" and "lean" indicate the corresponding flame case.

Flame 1 (ϕ = 0.67 and T = 1768 K) and Flame 5 (ϕ = 1.12 and T = 1843 K) were used to evaluate the absorption cross-section of KOH at ∼1800 K. The absorbance curves in these two flames obtained with seeding of the same amount of K_2CO_3 are presented in Figure 5a. A detailed description of the absorption spectrum of KOH is provided by Weng et al.[23] Absorption of the OH radical (∼283 and 310 nm) and K atoms (∼404 nm, 345 and 322 nm) can be observed, but are much narrower than that of KOH. The absorbance of KOH in the lean case nearly doubles the one in the rich case (cf. Figure 5a) and the difference was mainly caused by the difference in KOH concentration between these two cases. The influence of the temperature difference

DOI: 10.1021/acs.analchem.9b00203
Anal. Chem. 2019, 91, 4719−4726

between these two cases (1768 K vs 1843 K) is negligible, as reported by Weng et al.[23] The measured number densities of K atoms in Flames 1 and 5 were 1.7×10^{18} m^{-3} and 4.87×10^{19} m^{-3}, respectively. Thus, the absorption cross-section of KOH at a temperature of ~1800 K, as shown in Figure 5b, was obtained with eq 9, and is equal to 1.1×10^{-21} m^2/molecule at 327.3 nm and 1.29×10^{-21} m^2/molecule at 246.2 nm. Note that, by combining eqs 8 and 9, one can find that the path length L can be cancelled to obtain the cross-section values. In addition, the absorption cross-section of KOH at a temperature of ~1400 K was evaluated from measurements made in Flame 8 (ϕ = 0.67 and T = 1390 K) and Flame 10 (ϕ = 1.31 and T = 1471 K). The obtained absorption cross-section is presented in Figure 5b and has a value of 1.05×10^{-21} m^2/molecule at 327.3 nm and 1.26×10^{-21} m^2/molecule at 246.2 nm. It is about twice that used by Sorvajärvi et al.[17] near 320 nm, where it was approximated to the cross-section of NaOH reported by Self and Plane.[37] To the best of our knowledge, Figure 5b presents the first experimental data on the UV absorption cross-section of KOH. Comparing the two absorption cross-section profiles of KOH at temperatures around 1400 and 1800 K, it can be seen that the influence of temperature is small. The average value of the cross sections at temperatures 1400 and 1800 K was therefore applied in the calculation of the concentration of KOH in the following evaluation.

Furthermore, the UV absorption cross-section of KCl in the high-temperature gas was obtained. In order to generate KCl in the hot flue gas, $CHCl_3$ was seeded into the premixed flame as the source of chlorine. In the fuel-lean cases, with the seeding of K and Cl, the dominant potassium species in the hot flue gas were KOH and KCl, while <2.5% of the potassium formed K atoms, according to the measured concentration of K atoms and the total potassium concentration obtained in the case without the seeding of Cl. Especially in the low-temperature case, Flame 9, there were almost no K atoms present. Hence, the potassium balance is mainly between KOH and KCl. In the present investigations, ~100 ppm of Cl was introduced into the flame while the concentration of elemental potassium was maintained at ~20 ppm. It was observed that there was almost no KOH formed with the seeding of 100 ppm of Cl, according to the structure of the absorption spectrum, as shown in Figure 6a. Similar results have been presented by Schofield[38] on sodium chemistry and showed that NaCl became the dominant species as chlorine was available in excess compared with sodium. The absorption was solely from KCl, as it shows the same profile as the ones presented in previous studies on the UV absorption of KCl.[18−20,23] Consequently, the UV absorption cross-section of KCl was obtained based on the Beer−Lambert law with the measured absorbance of KCl in the flame (Figure 6a) and its corresponding concentration from the measured concentration of KOH under the condition without Cl seeding.

$$N_{\text{KOH-lean}} = N_{\text{KCl-lean}} = \frac{A_{\text{KCl-lean}}(\lambda)}{\sigma_{\text{KCl-lean}}(\lambda) \times L} \tag{10}$$

Figure 6b shows the absorption cross-section of KCl at temperatures of ~1800 and 1300 K with values of 2.3×10^{-21} m^2/molecule and 2.26×10^{-21} m^2/molecule, respectively, at a wavelength of 246.2 nm. The variation of the cross-section with temperature is shown to be small, as concluded by Leffler et al.[20] In the following, the value of 2.28×10^{-21} m^2/molecule at a wavelength of 246.2 nm was used in the KCl concentration evaluation. The present value is ~20% lower than the value from Leffler et al.[20] measured at a temperature of ~1000 K, which is ~28% higher than the values from Davidovits et al.[19] and Forsberg et al.[18] at a temperature of ~1100 K. In the measurements by Leffler et al.[20] and Davidovits et al.,[19] sealed quartz cells generating controlled amounts of KCl vapor were used, in which the evaluation of the KCl cross sections strongly relied on the determination of the KCl vapor pressure in the cell. The accuracy of the calculated KCl vapor pressure was directly affected by the accuracy of the salt reservoir temperature.[20] A possible uncertainty in measured temperature of 15 K could cause an uncertainty in vapor pressure of more than 20%.[20] Moreover, since a nearly saturated KCl vapor was generated in the cell, there might be some additional uncertainty induced by the formation of K_2Cl_2, as discussed by Leffler et al.[20] Compared with previous investigations, there are thus some advantages in the present study. First, the measurement was made directly on the KCl vapor in the combustion environment, in which the formation of the K_2Cl_2 dimer was negligible at temperatures over 1300 K. Also, the evaluation of the absorption cross-section was based on the measurement of the concentration of atomic K, which had a relatively low uncertainty. According to the estimation of the error in the absorbance curve-fitting process, the uncertainty was about ±2%. In addition, about ±3% uncertainty can be introduced by the uncertainty of around ±50 K in the TLAF temperature measurement of the hot gas. In addition, uncertainty might originate from the inhomogeneity of the potassium distribution in the hot flue gas. The inhomogeneity was estimated through the distribution of the photofragmenation fluorescence of KOH/KCl in the hot flue gas. The fluctuation of the concentration of potassium in the measurement region was estimated to be below ±10%. Moreover, under the rich condition, the secondary reactions occurred with the ambient air to form a thin layer of flame front, which might change the balance between KOH and K atoms. This influence should be small considering the fact that the reaction zone was very small with a thickness of <1% of the entire homogeneous reaction zone. However, combining eqs 8 and 9, it can be found that the path length L can be canceled and there was almost no influence on the determination of the absorption cross section. Hence, the total error of the absorption cross section was estimated to be about ±5% in the present study, without considering uncertainties in path length, inhomogeneity of temperature, and possible secondary reactions.

Concentration Measurements of K Atoms, KOH, and KCl in Flames. Quantitative measurements of KOH, KCl, and atomic K were performed to study the potassium−chlorine chemistry. To mimic different oxidation and reduction environments, hot flue gases were prepared from flames (Flames 1−7) with global equivalence ratios that varied from 0.67 to 1.32. A constant amount of KCl was seeded into the flames via KCl water solution. The concentrations of KOH, KCl, and K atoms measured through broadband UV absorption spectroscopy and TDLAS are shown in Figure 7 with a total amount of potassium being ~22 ppm.

It is clear that there is a significant change of the concentration for all the potassium species as the equivalence ratio varies from lean to rich cases. For the lean cases, the concentrations of different potassium species are almost kept constant. The KCl concentration was ~12 ppm, and the KOH had concentration of ~10 ppm. For the lean cases, the concentration of K atoms was measured both by the 404.4 nm and the 769.9 nm TDLAS system. The results obtained from these two methods agreed

DOI: 10.1021/acs.analchem.9b00203
Anal. Chem. 2019, 91, 4719−4726

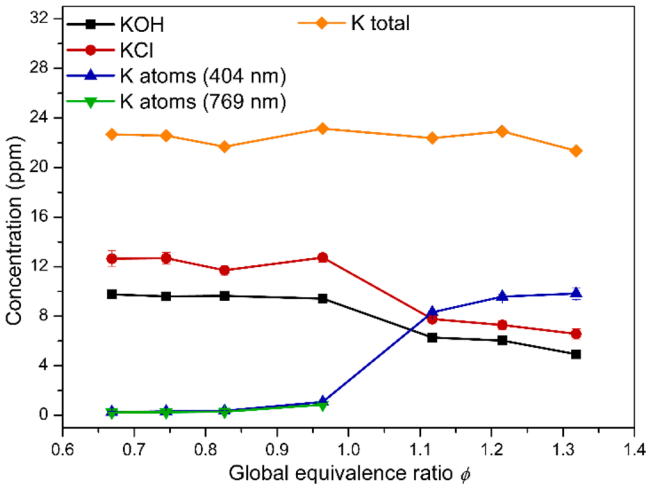

Figure 7. Concentration of K atoms, KOH, KCl, and total K in the hot flue gas versus global equivalence ratio with seeding of KCl. The concentration of K atoms was measured by TDLAS both at 404.4 and 769.9 nm in the fuel-lean cases. Note: the concentration in different cases was corrected due to the difference in total flow rate shown in Table 1.

well, both giving a value of ~0.3 ppm, which was much smaller than the concentrations of KCl and KOH. It can be seen that there was only ~1% potassium present in the form of K atoms in the oxidation environment at a temperature of 1800 K, while KCl and KOH concentrations constituted ~55% and ~43%, respectively, of the total potassium. In the reduction environments, the concentration of K atoms increased to 8 ppm, and continually increased with equivalence ratio. The fraction of K atoms became over 35% in reduction environments, in agreement with results presented by Leffler et al.,[15] indicating that K atoms should be considered as one of the dominant species in the reduction environment together with KCl and KOH, which had a fraction of 37% and 28%, respectively. The formation of large amounts of K atoms might be caused by the existence of a large amount of H radicals in the reduction environments, which enhanced reactions between KCl/KOH and H radicals.[26,39] The ratio between the concentration of KOH and the sum of KOH and KCl values was almost constant, even in the fuel-rich flames, which indicates that chemical equilibrium between KOH and KCl can be easily established.

CONCLUSIONS

In the present work, spectrally resolved UV absorption cross sections of KOH and KCl in the wavelength range 200−480 nm and at temperatures 1300 K and 1800 K were, for the first time, obtained directly through a reliable experimental method. The well-recognized spectral features make it possible to perform simultaneous KOH and KCl measurement in combustion environments. Meanwhile, the concentration of K atoms was measured using TDLAS combining the absorption lines at 769.9 and 404.4 nm to cover a dynamic range of concentrations from several ppb up to 20 ppm for a path length of 10 cm. Hence, all the major potassium species, i.e., KOH, KCl, and K atoms, present in most biomass combustion/gasification atmospheres, can be measured quantitatively. Using our experimental setup, a constant amount of KCl was seeded into flames with varying equivalence ratios and the concentrations of KOH, KCl, and K were measured. The chemical balance between different potassium species in different environments was accurately determined. These quantitative techniques can be used for accurate investigations of potassium chemistry and for potassium species monitoring in biomass combustors and gasifiers.

AUTHOR INFORMATION

Corresponding Author

*E-mail: zhongshan.li@forbrf.lth.se.

ORCID

Zhongshan Li: 0000-0002-0447-2748

Notes

The authors declare no competing financial interest.

ACKNOWLEDGMENTS

This work was financed by the Swedish Energy Agency (GRECOP, No. 38913-2), the Knut & Alice Wallenberg foundation (KAW 2015.0294, ALADIN), the Swedish Research Council (VR) and the European Research Council (ERC, No. 669466/TUCLA).

REFERENCES

(1) Johansen, J. M.; Jakobsen, J. G.; Frandsen, F. J.; Glarborg, P. *Energy Fuels* **2011**, *25*, 4961−4971.
(2) Zhao, H.; Song, Q.; Wu, X.; Yao, Q. *Energy Fuels* **2015**, *29*, 6404−6411.
(3) Huang, Y.; Liu, H.; Yuan, H.; Zhuang, X.; Yuan, S.; Yin, X.; Wu, C. *Energy Fuels* **2018**, *32*, 9605.
(4) Nielsen, H. P.; Frandsen, F. J.; Dam-Johansen, K.; Baxter, L. L. *Prog. Energy Combust. Sci.* **2000**, *26*, 283−298.
(5) Mason, P. E.; Darvell, L. I.; Jones, J. M.; Williams, A. *Fuel* **2016**, *182*, 110−117.
(6) Fatehi, H.; He, Y.; Wang, Z.; Li, Z. S.; Bai, X. S.; Aldén, M.; Cen, K. F. *Proc. Combust. Inst.* **2015**, *35*, 2389−2396.
(7) Weng, W.; Gao, Q.; Wang, Z.; Whiddon, R.; He, Y.; Li, Z.; Aldén, M.; Cen, K. *Energy Fuels* **2017**, *31*, 2831−2837.
(8) Liu, Y.; Wang, Z.; Xia, J.; Vervisch, L.; Wan, K.; He, Y.; Whiddon, R.; Bahai, H.; Cen, K. *Proc. Combust. Inst.* **2019**, *37*, 2681.
(9) Hsu, L.; Alwahabi, Z. T.; Nathan, G. J.; Li, Y.; Li, Z. S.; Aldén, M. *Appl. Spectrosc.* **2011**, *65*, 684−691.
(10) He, Y.; Zhu, J.; Li, B.; Wang, Z.; Li, Z.; Aldén, M.; Cen, K. *Energy Fuels* **2013**, *27*, 1123−1130.
(11) Oldenborg, R. C.; Baughcum, S. L. *Anal. Chem.* **1986**, *58*, 1430−1436.
(12) Leffler, T.; Brackmann, C.; Aldén, M.; Li, Z. *Appl. Spectrosc.* **2017**, *71*, 1289−1299.
(13) Leffler, T.; Brackmann, C.; Berg, M.; Li, Z.; Aldén, M. *IFRF Combust. J.* **2016**, *2016*, 1−19.
(14) Leffler, T.; Brackmann, C.; Berg, M.; Aldén, M.; Li, Z. *Energy Procedia* **2017**, *120*, 365−372.
(15) Leffler, T.; Brackmann, C.; Weng, W.; Gao, Q.; Aldén, M.; Li, Z. *Fuel* **2017**, *203*, 802−810.
(16) Qu, Z.; Steinvall, E.; Ghorbani, R.; Schmidt, F. M. *Anal. Chem.* **2016**, *88*, 3754−3760.
(17) Sorvajärvi, T.; DeMartini, N.; Rossi, J.; Toivonen, J. *Appl. Spectrosc.* **2014**, *68*, 179−184.
(18) Forsberg, C.; Broström, M.; Backman, R.; Edvardsson, E.; Badiei, S.; Berg, M.; Kassman, H. *Rev. Sci. Instrum.* **2009**, *80*, 023104.
(19) Davidovits, P.; Brodhead, D. C. *J. Chem. Phys.* **1967**, *46*, 2968−2973.
(20) Leffler, T.; Brackmann, C.; Berg, M.; Aldén, M.; Li, Z. S. *Rev. Sci. Instrum.* **2017**, *88*, 023112.
(21) Rowland, F. S.; Makide, Y. *Geophys. Res. Lett.* **1982**, *9*, 473−475.
(22) Daidoji, H. *Bunseki Kagaku* **1979**, *28*, 77−82.
(23) Weng, W.; Leffler, T.; Brackmann, C.; Aldén, M.; Li, Z. *Appl. Spectrosc.* **2018**, *72*, 1388−1395.

DOI: 10.1021/acs.analchem.9b00203
Anal. Chem. 2019, 91, 4719−4726

(24) Babushok, V. I.; Linteris, G. T.; Hoorelbeke, P.; Roosendans, D.; van Wingerden, K. *Combust. Sci. Technol.* **2017**, *189*, 2039−2055.
(25) Carabetta, R.; Kaskan, W. E. *J. Phys. Chem.* **1968**, *72*, 2483−2489.
(26) Slack, M.; Cox, J. W.; Grillo, A.; Ryan, R.; Smith, O. *Combust. Flame* **1989**, *77*, 311−320.
(27) Weng, W.; Borggren, J.; Li, B.; Aldén, M.; Li, Z. *Rev. Sci. Instrum.* **2017**, *88*, 045104.
(28) Stull, D. R. *Ind. Eng. Chem.* **1947**, *39*, 517−540.
(29) Xieqi, M.; Cicek, B.; Senkan, S. M. *Combust. Flame* **1993**, *94*, 131−145.
(30) Li, Z. S.; Sun, Z. W.; Li, B.; Aldén, M.; Försth, M. *Opt. Lett.* **2008**, *33*, 1836−1838.
(31) Borggren, J.; Weng, W.; Hosseinnia, A.; Bengtsson, P.-E.; Aldén, M.; Li, Z. *Appl. Phys. B: Lasers Opt.* **2017**, *123*, 278.
(32) Borggren, J.; Burns, I. S.; Sahlberg, A.; Aldén, M.; Li, Z. *Appl. Phys. B: Lasers Opt.* **2016**, *122*, 58.
(33) Schlosser, E.; Fernholz, T.; Teichert, H.; Ebert, V. *Spectrochim. Acta, Part A* **2002**, *58*, 2347−2359.
(34) Gao, Q.; Weng, W.; Li, B.; Li, Z. *Chin. Phys. Lett.* **2018**, *35*, 024202.
(35) van Eyk, P. J.; Ashman, P. J.; Alwahabi, Z. T.; Nathan, G. J. *Combust. Flame* **2008**, *155*, 529−537.
(36) Sansonetti, J. E. *J. Phys. Chem. Ref. Data* **2008**, *37*, 7−96.
(37) Self, D. E.; Plane, J. M. C. *Phys. Chem. Chem. Phys.* **2002**, *4*, 16−23.
(38) Schofield, K. *Combust. Flame* **2012**, *159*, 1987−1996.
(39) Li, B.; Sun, Z.; Li, Z.; Aldén, M.; Jakobsen, J. G.; Hansen, S.; Glarborg, P. *Combust. Flame* **2013**, *160*, 959−969.

DOI: 10.1021/acs.analchem.9b00203
Anal. Chem. 2019, 91, 4719−4726